Sci. Rep. RITU A42 (1996) pp. 239-244
No. 1, March 1996

New In-House Grazing Incident X-ray Scattering (GIXS) Apparatus for Studying Liquid Surface and Interface*

Shigeo Sato[a], Masatoshi Saito[a], Eiichiro Matsubara[b], Yoshio Waseda[a]

[a]*Institute for Advanced Materials Processing, Tohoku University, Sendai 980-77, Japan*
[b]*Department of Materials Science and Engineering, Graduate school, Kyoto University, Kyoto 606, Japan*

(Received December 28, 1995)

An in-house grazing incidence X-ray scattering (GIXS) apparatus has been newly built for studying a liquid surface and a liquid/solid or liquid/liquid interface. This apparatus consists of a high flux rotating anode x-ray generator, pairs of slits for incident and diffracted beams, a channel-cut Ge 440 crystal monochromator and a double-axis diffractometer. The capability of this system was tested by measuring the reflection profiles from a water surface and an interface of water and mercury-electrode.

Keywords : GIXS, x-ray reflectivity, liquid surface, liquid/liquid interface

1. Introduction

The grazing incident x-ray scattering (hereafter, referred to as GIXS) method has been applied for studying surface structures of various substances. Density profiles and other features of the surface have been deduced in solid films[1) ~ 4)], liquid crystals[5) ~ 7)] and water[8)] by analyzing deviation of an experimental reflectivity curve from Fresnel's reflection. An in-plane atomic structure of a solid or liquid surface has also been determined by measuring the out-of-reflection-plane diffraction under the total external reflection condition[9)]. Similarly, an interface structure with different refractive indices has also been obtained by totally refracting x-ray beams at the interface[10)].

We are specially interested in the structure of the electrode-solution interface. Its interface structure has been studied[11) 12)] and some models for the interface have been proposed[13) 14)]. Very recently, the atomic force microscopy (AFM) study has also been done on the electrode-solution interface[15)].

In this paper, we will describe our in-house GIXS apparatus which has been recently built for the structural study of the surface of solution and the electrode-solution interface. The reflection profiles of water and water-mercury-electrode interface observed in this apparatus will be shown.

2. Experimental

Only the way to measure the reflection from the liquid surface or liquid/liquid interface is that the GIXS geometry should be arranged horizontally. Thus, we must devise the method to irradiate the x-ray beams to the horizontal liquid surface with a small glancing angle. Since a high-flux rotating anode generator is used as the x-ray source, to tilt the x-ray target is not a practical solution. Fortunately, the glancing angle necessary for the GIXS measurement in the present study is at most about 0.4° (≅7mrad) and the divergence from the point focus of the target is much larger. Thus, by decreasing the heights of two slits S_1 and S_2 located on the stage supported by two elevators Z_1 and Z_2 in Fig. 1, a part of a relatively large divergent beam from the target is incident on a horizontal liquid surface with a precise glancing angle. Similarly, the take-off angle of the reflected beam or the surface diffraction, α', is defined by two slits S_4 and S_5 whose height is adjusted by two elevators Z_4 and Z_5 in Fig. 1. The sample cell was mounted on a double crossed swivel stage which is attached on the elevator Z_3 in Fig. 1. By changing the sample height so that the incident beam can irradiate the center of the sample with the glancing angle of α and α' for the incident and reflected beams. These elevators are moved by stepping motors whose finest step is 0.25 μm. Thus, the accuracy of the values of α and α' are 1.4×10^{-3} mrad and 0.63×10^{-3} mrad, respectively.

The rotating anode x-ray generator (Rigaku RU-300) with a molybdenum target and a high brilliant filament is operated at 4kW. Monochromatic Mo Kα radiations are obtained with a channel-cut Ge 440 crystal. In this way, the monochromatic and incident beams are made parallel each other. The intensity of this monochromatic Mo Kα radiation measured at various incident angles from 0 to 12.2 mrad is

* The 96-R1 report of Institute for Advanced Materials Processing (SOZAIKEN)

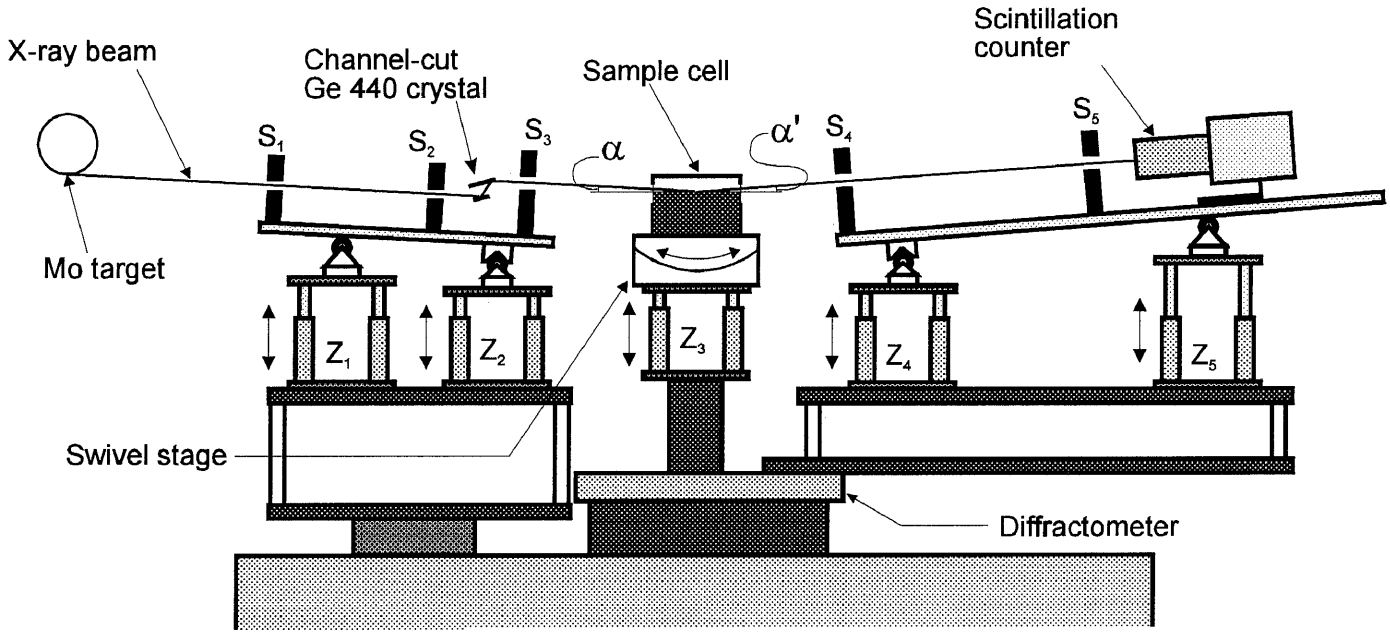

(a)

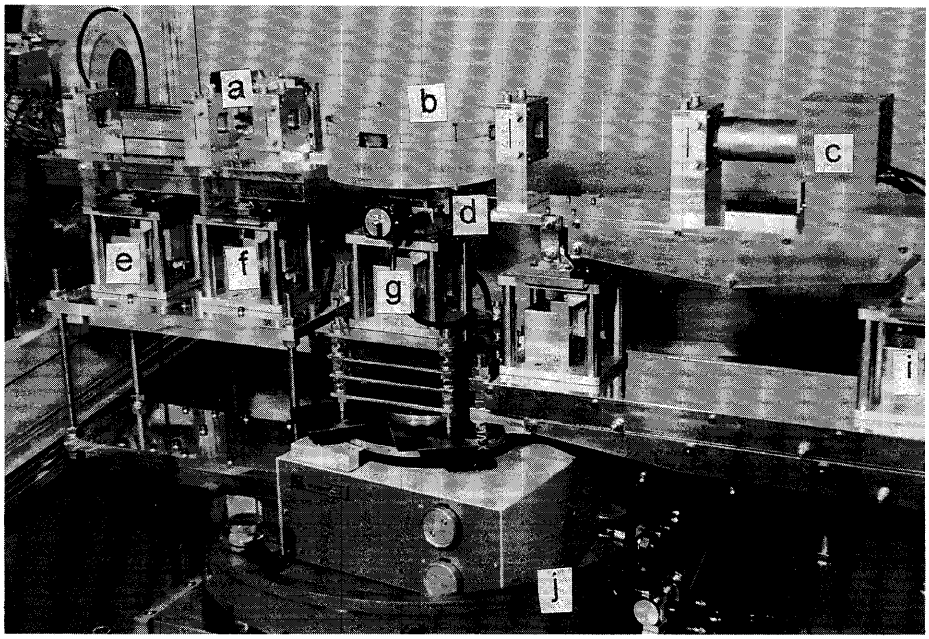

(b)

Fig. 1 (a) Schematic diagram of the geometry for x-ray diffraction from a horizontal fluid surface and (b) its overview: a. the channel cut Ge 440 crystal, b. the sample cell, c. the scintillation counter, d. the swivel stage, e~i. the elevators, j. the diffractometer.

shown in Fig. 2. It is easily seen that the intensity distribution of the divergent beam is quite homogeneous in the range of the present measurement.

The counter arm holding the two elevators and slits, and the counter rotates round the center of the sample stage. This enables us to observe the scattering from the surface or interface. Scattering x-ray intensity detected by a scintillation counter is energetically discriminated by a single channel analyzer. The signals from the single channel analyzer are read by the micro-computer through the counter-timer with the GPIB interface. Since this counter-timer has two channels for inputs, the two signals of different energies can be observed simultaneously. The schematic diagram of the arrangements of the electronics in the present system are explained in the Fig. 3. The movements of elevators and a swivel stage are independently driven by stepping motors. These stepping motors are also controlled by the micro-computer as it is schematically explained in Fig. 4. The program for control of the present system is written in Microsoft Quick-BASIC.

It is worth mentioning that the vibrations of liquid surface in the present system is extremely reduced by using a box of sand and, alternately stacked rubber sheets and steel plates as an absorber.

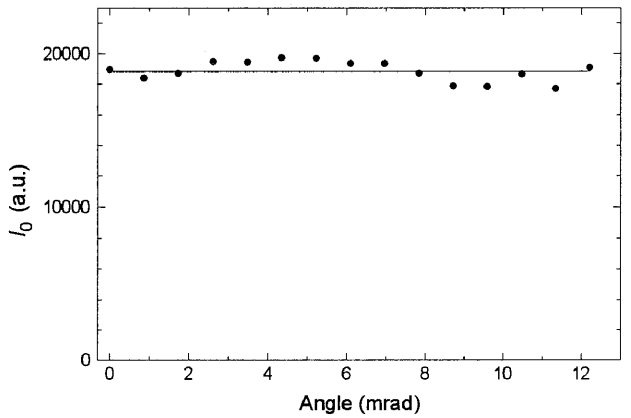

Fig. 2 The incident x-ray intensity distribution from 0mrad to 12.2mrad.

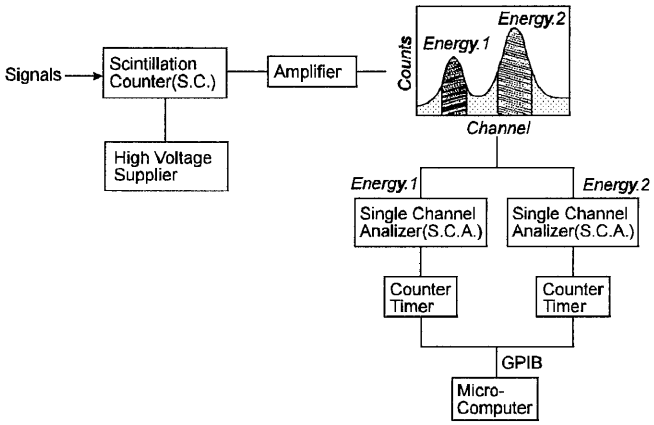

Fig. 3 Schematic diagram of arrangements of the associated electronics.

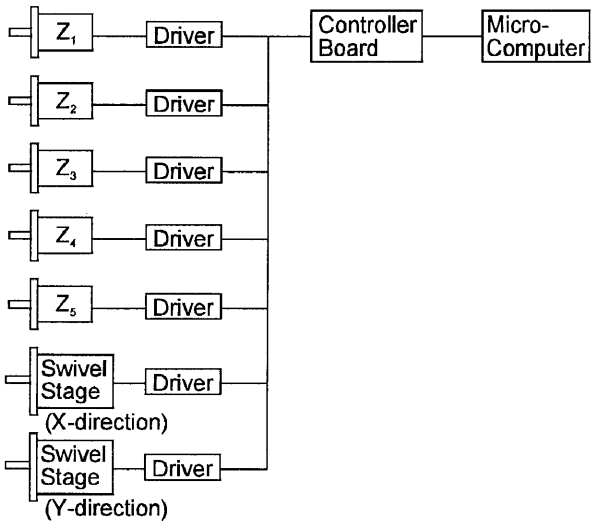

Fig. 4 Schematic diagram of pulse-motor control system.

3. Theoretical Background

We consider the reflection and refraction at a planar interface where the index of refraction changes abruptly from n_j to n_{j+1} as it is schematically shown in Fig. 5. The theoretical calculation of reflectivity for such a multilayer has been carried out by L. G. Parratt[16]. In his calculation, the reflection and transparence of x-ray beams at the interface are considered. The complex refractive index n of a substance in the layer j ($0 \leqq j \leqq N$) for x-rays is given by

$$n_j = 1 - \delta_j - i\beta_j . \qquad (1)$$

where

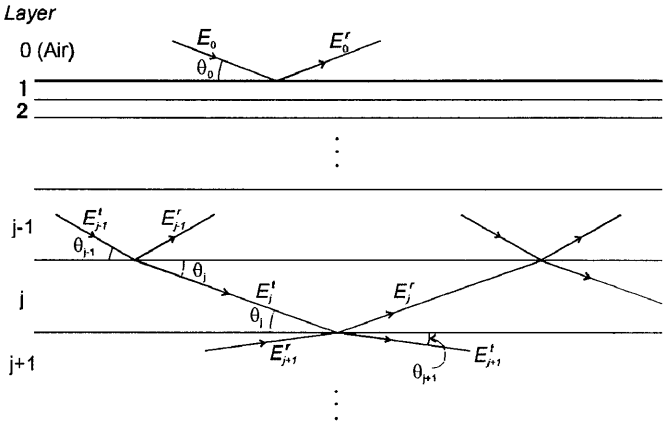

Fig. 5 Representation of a multilayered stack consisting of homogeneous layers. θ_i is the refracted angle in the layer i. E_i^t and E_i^r are the transmitted and reflected electric fields in the layer i, respectively.

$$\delta_j = \frac{N_A}{2\pi}\frac{\rho_j}{M_j}(f_{0j} + f_j')r_e\lambda^2, \tag{2}$$

$$\beta_j = \frac{N_A}{2\pi}\frac{\rho_j}{M_j}f_j''r_e\lambda^2 = \frac{\mu_j\lambda}{4\pi}, \tag{3}$$

and

$$f_j = f_{0j} + f_j' + i f_j'', \tag{4}$$

The subscript of j indicates j-layer. N_A is Avogadro's number, ρ_j the density, M_j the atomic weight, r_e the classical electron radius, λ the wavelength, μ_j the linear absorption coefficient and f_j the complex atomic x-ray scattering factor. The terms of f_{0j}, f'_j and f''_j are the normal x-ray atomic scattering factor and the real and imaginary parts of the anomalous dispersion terms, respectively.

When the transparent wave in the layer j-1 travels to the layer j, the relation between the incidence angle θ_{j-1} and the refracted angle θ_j of the transmitted wave is written by Snell's law.

$$n_j = \frac{\cos\theta_{j-1}}{\cos\theta_j} = \frac{\prod_{k-1}^{j-1} n_k \cos\theta_0}{\cos\theta_j}. \tag{5}$$

As the refractive index for x-rays is almost unity, $\prod_{k-1}^{j-1} n_k \cong 1$. Therefore,

$$n_j \cong \frac{\cos\theta_0}{\cos\theta_j}. \tag{6}$$

Since the deviation of n_j from unity is very small, appreciable refraction occurs only for a very small angle. Thus, the cosine term is expanded, i.e. $\cos\theta_j \cong 1-\theta_j^2/2$. In addition, for x-rays, $\delta_j \ll 1$, and $\beta_j \ll 1$ for the angle around total reflection condition. From eqs. (1) and (6)

$$\theta_j = \sqrt{\theta_0^2 - 2\delta_j - 2i\beta_j}. \tag{7}$$

The continuity of the tangential components of the electric vectors for the boundary of the layers j-1and j in Fig. 5 is expressed by

$$a_{j-1}E_{j-1}^t + a_{j-1}^{-1}E_{j-1}^r = a_j^{-1}E_j^t + a_j E_j^r, \tag{8}$$

and

$$(a_{j-1}E_{j-1}^t - a_{j-1}^{-1}E_{j-1}^r)\theta_{j-1}k_1 = (a_j^{-1}E_j^t - a_j E_j^r)\theta_j k_1, \tag{9}$$

where

$$a_j = \exp(-i k_1 \theta_j \frac{d_j}{2}) = \exp(-i\frac{\pi}{\lambda}\theta_j d_j). \tag{10}$$

The term of d_j is the thickness of the j-layer. In eqs. (8) and (9), the amplitudes of vectors E_{j-1}^r, E_j^t and E_j^r refer to the values midway through medium j-1 and j, respectively.

The solution of the simultaneous eqs. (8) and (9) is obtained by dividing their difference through their sum and writing the result as a recursion formula

$$R_{j-1,j} = a_{j-1}^4 \frac{R_{j,j+1} + F_{j-1,j}}{R_{j,j+1}F_{j-1,j} + 1}, \tag{11}$$

where

$$R_{j,j+1} = a_j^2 \frac{E_j^r}{E_j^t}. \tag{12}$$

$F_{j,j+1}$ is the Fresnel coefficient for reflection at the interface between layer j and j+1 and given by

$$F_{j,j+1} = \frac{\theta_j - \theta_{j+1}}{\theta_j + \theta_{j+1}}. \tag{13}$$

Eq. (13) is solved by the boundary condition for the layer N whose thickness is infinite, i.e. $R_{N,N+1} = 0$. Furthermore, a_1=1. Thus, in the present case, i.e. the water and mercury-electrode interface, $R_{1,2} = E_1^r / E_1$.

The ratio of reflected intensity to incident one, I_R/I_0, is obtained by separating $R_{1,2}$ in eq. (11) into its real and imaginary terms and multiplying by its complex conjugate. The x-ray reflectivity is evaluated from the following relation;

$$\frac{I_R}{I_0} = \left|\frac{E_0^R}{E_0}\right|^2. \tag{14}$$

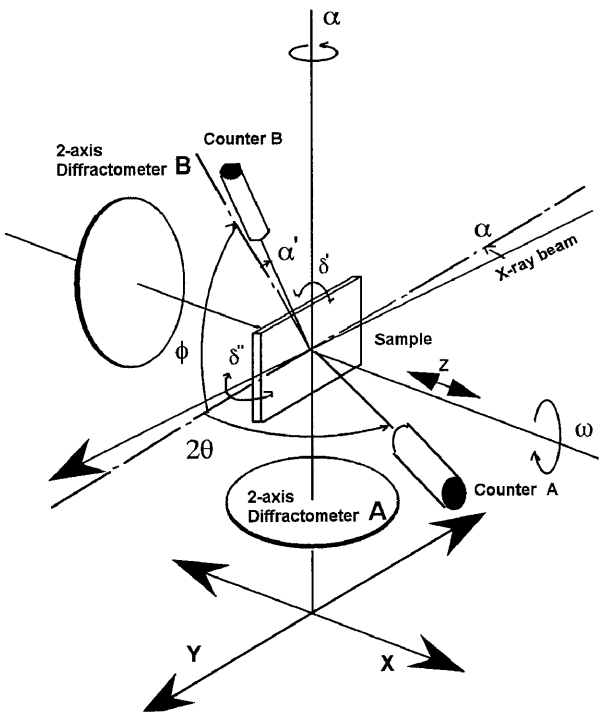

Fig. 6 Schematic diagram of configurations of rotation axes equipped in the crossed double-axis diffractometer.

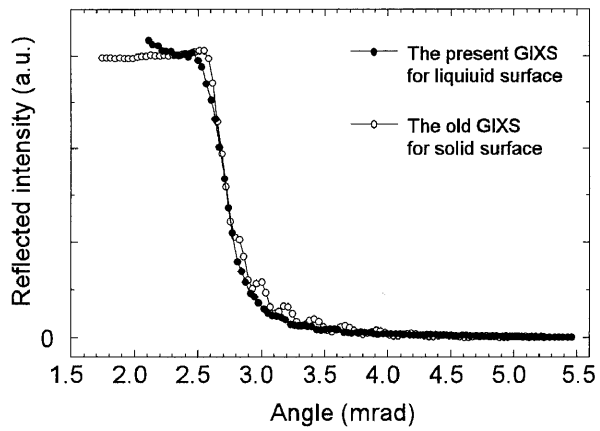

Fig. 7 Experimental reflection curves of Fe_2O_3 film on Si wafer measured with the new GIXS apparatus (solid circles) and the usual GIXS apparatus (open circles).

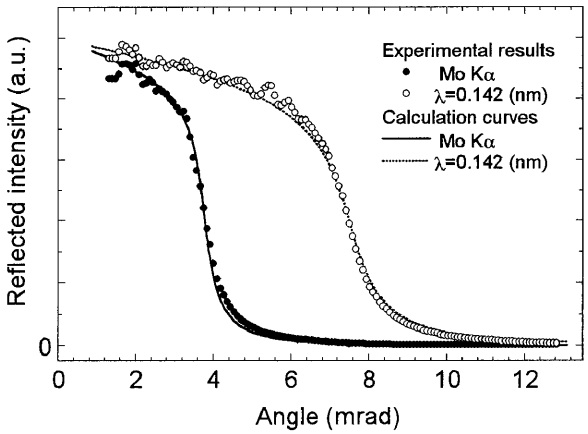

Fig. 9 Experimental reflection curves of mercury surface observed with Mo Kα (λ=0.071nm) (solid circles) and the white x-ray (λ=0.142nm) (open circles) monochromated by Ge 220. Solid curve (Mo Kα) and dotted curve (white x-ray) are the calculated ones.

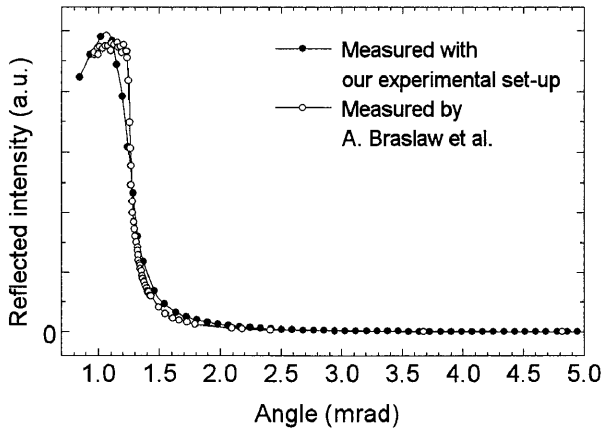

Fig. 8 Experimental reflection curves of water surface measured with our apparatus (solid circles) and by A. Braslaw[8] (open circles).

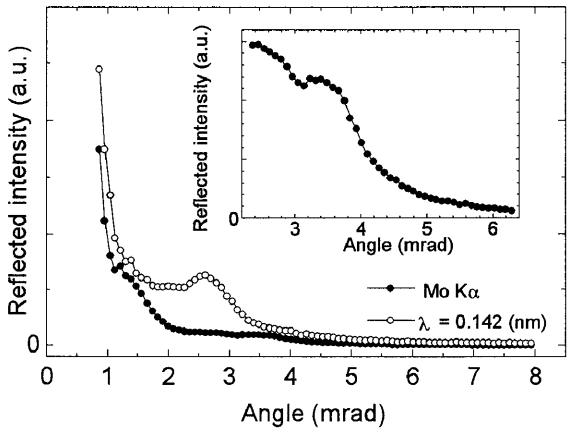

Fig. 10 Experimental reflection curves of Kapton/water/mercury sample observed with Mo Kα (λ=0.071nm) (solid circles) and the white X-ray (λ=0.142nm) (open circles). The inset shows expanded profiles for Mo Kα.

4. Results and Discussion

In another in-house GIXS system in Fig. 6 which has been built in our laboratory, an incident angle is adjusted by rotating the sample around the axis including the surface, i.e. the α-axis in Fig. 6. In the present system, however, this glancing angle to the sample surface can be selected by adjusting the heights of the slits and sample as it is explained in the previous section. Namely, the incident angle in the present system is controlled by the completely different method. In order to test the accuracy of incident angles, the reflectivity curves of Fe_2O_3 film grown on Si wafer were observed in each in-house GIXS diffractometer. Two reflectivity curves are given in Fig. 7. These curves gives the same critical angle of Fe_2O_3 film. In the present system, the monochromatic Mo Kα radiation is obtained by 440 reflection of the channel-cut Ge crystal while Ge 111 single crystal plate is used in another system. Thus, in spite of better energy resolution, the incident intensity is extremely reduced in the present system. In the actual measurement in the present system, the energy resolution is slightly not strict to make up for the decrease in the incident intensity. This is clearly seen in the oscillations above α=3 mrad which is due to interference of reflected x-rays by the surface of the Fe_2O_3 film and the interface between the film and Si wafer. From these observations, it is reasonably concluded that the present GIXS system works well and considered as reliable as that in another one.

The reflectivity of water surface observed in the present system is compared with that reported by Braslaw et al[8]. in Fig. 8. The critical angle of the reflectivity curves

almost agrees with each other. This result confirms the ability of the present system for measuring the reflectivity profile from the liquid surface. The sharpness of reflectivity curve is not as good as that by Braslaw's case. This may be caused by the small curvature of the water surface arising from the small cell size in the present study. Thus, the use of larger cell was suggested in the measurement for the water-mercury-electrode interface.

It is well known that the mercury-electrode is a typical polarizable electrode. This is appropriate to investigate a relation between the interface structure and applied voltage to the electrode. First, the reflectivity profile from mercury was measured. The reflectivity profiles of mercury for Mo Kα (0.071 nm) diffracted by Ge 440 and for the two times larger wavelength of 0.142 nm by Ge 220 were observed simultaneously. They are shown in Fig. 9. The critical angle for Mo Kα is 3.7 mrad, which indicates the surface density of mercury is 13.4 g/cm^3. This value is very close value of pure mercury, 13.5 g/cm^3. Furthermore, the critical angle of mercury for 0.142 nm is twice as large as that for Mo Kα, which satisfies the proportional relation between the critical angle and the wavelength. This result also demonstrates the accuracy of the angular setting for incident beams in the present system.

Since the incident and reflected x-ray beams are absorbed by water in measuring the reflectivity at the interface between water and mercury, the thickness of water layer on mercury should be as thin as possible. However, since the wettability of mercury to water is very bad, it is difficult to cover mercury surface with a thin water layer. In the present study, the water layer is sandwiched by mercury and a Kapton film. In this way, the thin and uniform water layer was achieved. The reflective profile of Kapton/water/mercury sample is shown in Fig. 10. In this measurement, the profiles for two wavelengths of 0.071 nm (Mo Kα) and 0.142 nm were obtained. The reflected intensity for Mo Kα decreases rapidly at about 1 mrad and gradually decays up to 2 mrad. A similar profile is detected for 0.142 nm at just two times larger scattering angles than those for Mo Kα. The decrease of the reflective profile for water covered by the Kapton film becomes broader than that measured for a free water surface in Fig. 8. This is because the Kapton film on water was not perfectly flat. The reflected intensity decreases again at about 3.7mrad. Though this decrease is very small, this is ascribed to the reflection at the interface between water and mercury. These measurements clearly demonstrate that the new GIXS apparatus enables us to measure the scattering from the water-mercury-electrode interface.

There are few applications of the GIXS method to the structural studies of the liquid-liquid interface. In this paper, we have demonstrated some measurements from the water surface and the water-mercury-electrode interface, using our new apparatus which has been specially built for the GIXS measurement for the liquid surface and interface, It is also found in these measurements that the intensity of the incident x-rays should be improved ; for example, the x-ray beam path is being replaced by He gas. Now we are continuing to do some further measurements in order to reveal the water-mercury-electrode interface with unknown structure.

Acknowledgments

This research is supported by Grant-in-Aid for Developmental Scientific Research B(2) (No.06555178).

References

1) M. Saito, T. Kosaka, E. Matsubara and Y. Waseda : Mater. Trans., JIM, **36** (1995) 1
2) W. C. Marra, P.E. Eisenberger and A. Y. Cho : J. Appl. Phys. , **50** (1979) 6928
3) G. Lim. W. Parrish, C. Ortiz, M. Bellotto, M. Hart : J. Mater. Res., **2** (1987) 471
4) A. Lieb, H. Dosch, J. H. Bilgram : Physica B, **198** (1994) 92
5) P. S. Pershan and J. Als-Nielsen : Phys. Rev. Lett., **52** (1984) 759
6) J. Als-Nielsen : Z. Phys. B-Condensed Matter, **61** (1985) 441
7) A. H. Weiss, M. Deutsch, A. Braslaw, B. M. Ocko, P. S. Pershan : Rev. Sci. Instrum., **57** (1986) 2554
8) A. Braslaw, M. Deutsch, P. S. Pershan, A. H. Weiss, J. Als-Nielsen and J. Boer : Phys. Rev. Lett., **54** (1985) 114
9) J. Als-Nielsen : Physica, **140A** (1986) 376
10) K. Akimoto, I. Hirosawa, T. Tatsumi, H. Hirayama, J. Mizuki and J. Mitsui : Appl. Phys. Lett., **56** (1990) 1225
11) Paik. W, Genshaw M.A., Bockris J. O'M. : J. Phys. Chem., **74** (1970) 4266
12) Murphy O.J., Pou T. E., Bockris J. O'M. : J. Electrochem. Soc., **131** (1984) 2785
13) Smart N. G., Bhardwaj R.C., Bockris J. O'M. : Corrosion, **48** (1992) 764
14) Bockris J. O'M. : Mater. Sci. & Eng. : **53** (1982) 47
15) Cruickshank B. J., Sneddon D. D., Gewirth A. A. : Surf. Sci., **281** (1993) L308
16) L. G. Parratt : Phys. Rev., **95** (1954) 359